ACS APPLIED MATERIALS & INTERFACES

www.acsami.org

Research Article

Embedded 3D Bioprinting of Gelatin Methacryloyl-Based Constructs with Highly Tunable Structural Fidelity

Liqun Ning, Riya Mehta, Cong Cao, Andrea Theus, Martin Tomov, Ning Zhu, Eric R. Weeks, Holly Bauser-Heaton, and Vahid Serpooshan*

Cite This: *ACS Appl. Mater. Interfaces* 2020, 12, 44563−44577

Read Online

ACCESS | Metrics & More | Article Recommendations | Supporting Information

ABSTRACT: Three-dimensional (3D) bioprinting of hydrogel-based constructs at adequate consistency and reproducibility can be obtained through a compromise between the hydrogel's inherent instability and printing fidelity. There is an increasing demand to develop bioprinting modalities that enable high-fidelity fabrication of 3D hydrogel structures that closely correspond to the envisioned design. In this work, we performed a systematic, in-depth characterization and optimization of embedded 3D bioprinting to create 3D gelatin-methacryloyl (gelMA) structures with highly controlled fidelity using Carbopol as suspension bath. The role of various embedded printing process parameters in bioprinting fidelity was investigated using a combination of experimental and theoretical approaches. We examined the effect of rheological properties of gelMA and Carbopol at varying concentrations, as well as printing conditions on the volumetric flow rate of gelMA bioink. Printing speed was examined and optimized to successfully print gelMA into the support bath at varying Carbopol concentrations. Printing fidelity was characterized in terms of printed strand diameter, uniformity, angle, and area. The optimal Carbopol solution that retained filament shape at highest fidelity was determined. The efficacy of developed bioprinting approach was then demonstrated by fabricating 3D hydrogel constructs with varying geometries and visualized using an advanced synchrotron-based imaging technique. We also investigated the influence of the Carbopol medium on cross-linking and the resulting stiffness of gelMA constructs. Finally, in vitro cytotoxicity of the developed bioprinting approach was assessed by printing human umbilical vein endothelial cells encapsulated in the gelMA bioink. These results demonstrate the significance of the close interplay between bioink−support bath rheology and printing parameters and help to establish an optimized workflow for creating 3D hydrogel structures with high fidelity and cytocompatibility via embedded bioprinting techniques. This robust platform could further expand the application of bioprinted soft tissue constructs in a wide variety of biomedical applications.

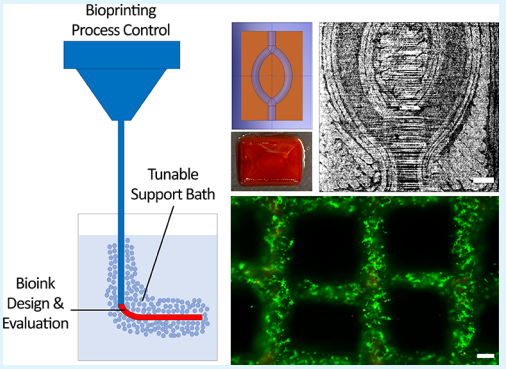

KEYWORDS: *3D embedded bioprinting, gelatin methacryloyl, gelMA, Carbopol, printing process control, structural fidelity, mechanical property, cytocompatibility*

INTRODUCTION

Hydrogels can trap large amounts of water, making them attractive candidates to provide biomimetic environments for living and functional cells.[1] Through extrusion-based three-dimensional (3D) bioprinting, hydrogels can be deposited with precise spatial control to form 3D structures that correspond to computer-aided design (CAD) models that have desirable properties.[2−4] Hydrogel prints have presented tremendous potential in biomedical engineering enhancing a wide range of applications.[5] Unfortunately, bioprinting of hydrogels is typically a race against material instability, due to the inherent flow behavior and their weak mechanical properties. Thus, 3D bioprinting of hydrogel constructs with adequate integrity and structural fidelity has been challenging, particularly in fabricating tissue constructs at large, clinical scales. This has resulted in a rapidly growing demand to develop new additive manufacturing methods that enable the assembly of hydrogel structures at acceptable fidelity and precision.

With no additional support for the bioink in extrusion bioprinting, the fidelity of bioprinted structures heavily relies on the properties of the hydrogel bioink, such as fluidic viscosity.[6] Greater viscosities are usually preferred to maintain 3D printed structures, but this typically requires larger quantities (concentrations) of the hydrogel material, resulting in excessive stiffness postpolymerization, which could in turn, significantly diminish the viability and function of encapsulated cells.[7] To enable

Received: August 20, 2020
Accepted: September 14, 2020
Published: September 23, 2020

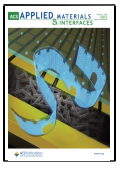

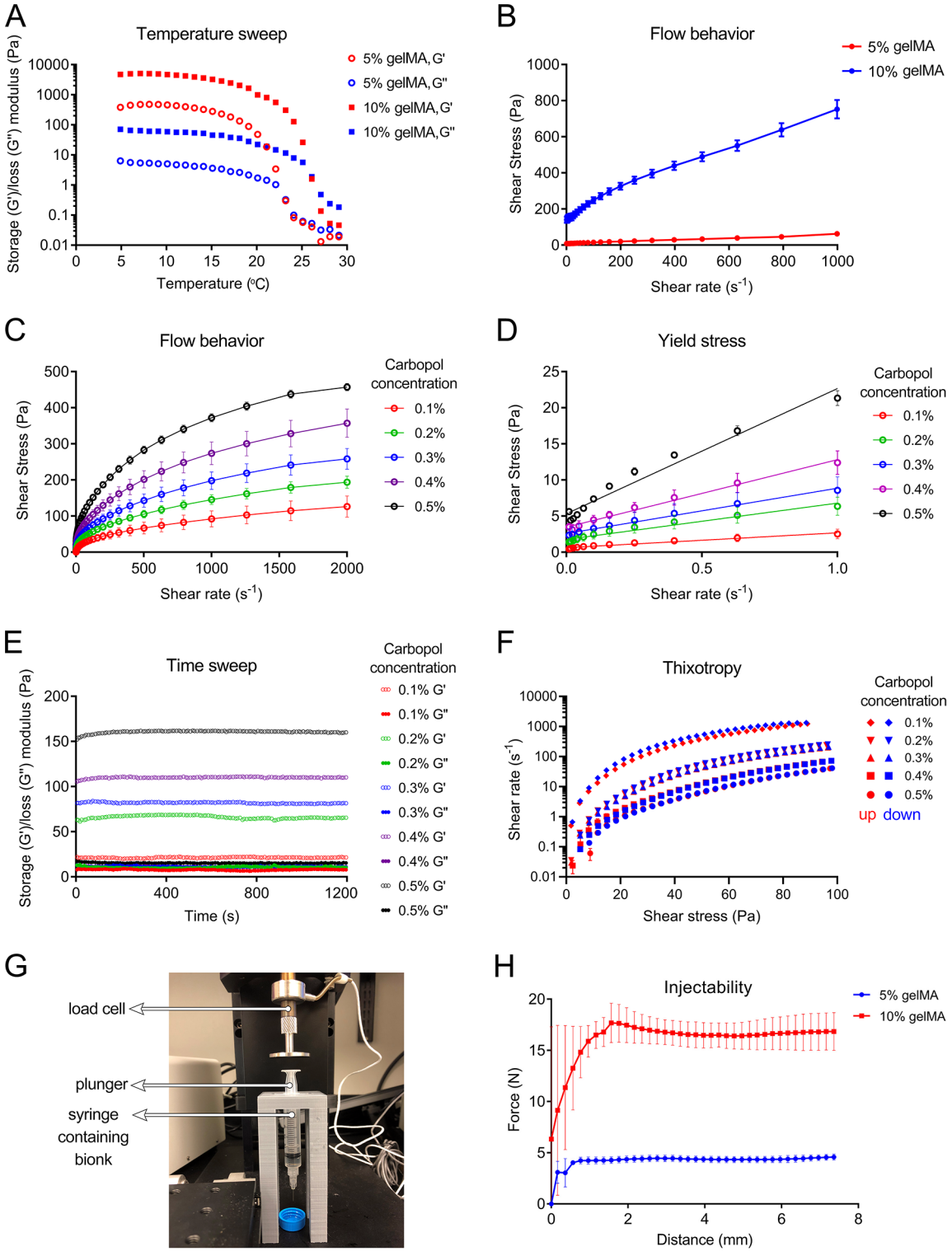

Figure 1. Characterization of gelMA and Carbopol solutions at varying concentrations. (A) Temperature sweep on 5 and 10% gelMA solutions through a cooling process from 30 to 5 °C. (B) Steady shear sweep on 5 and 10% gelMA at 23 °C. (C) Steady shear sweep on Carbopol solutions at concentrations ranging from 0.1 to 0.5% at 23 °C. (D) Yield stress measurement via a steady shear sweep using low shear rates from 0.01 to 1 s^{-1}. (E) A 20 min time sweep assay was performed on Carbopol solutions from 0.1 to 0.5% at 23 °C. (F) Thixotropy analysis on Carbopol solutions from 0.1% to 0.5% at 23 °C. (G) The experimental setup used for injectability measurement. (H) Injection force−distance curves for 5 and 10% gelMA at 23 °C.

bioprinting hydrogel inks at lower viscosities, 3D bioplotting, i.e., *printing while cross-linking*, has been utilized by extruding the precursor ink into a cross-linking bath.[8] While this method has somewhat addressed the issue of low-viscosity hydrogel printability, preparation of the cross-linking media requires meticulous and time-consuming adjustment steps, since the stability of the hydrogel during 3D stacking is highly sensitive to the cross-linking rate and the buoyancy of cross-linking media.[2,9] Another method developed to address hydrogel instability is hybrid printing, where a second ink is simultaneously deposited

https://dx.doi.org/10.1021/acsami.0c15078
ACS Appl. Mater. Interfaces 2020, 12, 44563−44577

to form a support frame that helps maintain the integrity of the soft hydrogel.[10,11] This printing approach faces some difficulties, however, to retain the printed hydrogel components while undergoing a liquid−solid phase change, which leads to compromised printing fidelity. Some hybrid printing efforts have employed sacrificial materials to improve structure fidelity and create complex structures such as vascular networks.[12,13] These multimaterial printing methods often introduce extra complexity and technical difficulties to achieve optimal print and postprint treatments for the combination of inks in use.

Embedded bioprinting has emerged as a promising alternative method that shows great promise for fabricating a wide variety of hydrogel-based structures while maintaining the desired structural stability and fidelity.[14,15] The difference between the embedded technique compared to other bioprinting techniques is the addition of a viscoplastic suspension bath. During embedded bioprinting, hydrogel precursor is extruded into a support material (bath) that undergoes shear thinning while maintaining a certain yield strength to preserve the dimensional stability of the printed bioink. Thus, it offers a paradigm alteration in 3D bioprinting by diminishing the need to compromise between material biomimicry and manufacturability.

Polyacrylic acid based Carbopol suspension has been used in 3D embedded bioprinting, allowing the precise printing of varying hydrogel types such as decellularized ECM (dECM), collagen, and fibrin, as well as the photo-cross-linkable poly(vinyl alcohol).[15] Carbopol exhibits stable, while tunable, viscoplastic behavior with a cell-friendly environment.[16] Compared to other support media, such as gelatin slurry and alginate microparticles,[14] Carbopol bath preparation is simpler and more efficient, and the printouts can be easily extracted through PBS (phosphate buffered saline) wash. While these advantages have been reported for the use of Carbopol support baths in bioprinting, there is yet not a systematic work conducted to date to elucidate the roles of the key parameters involved in such processes. In particular, the effects of Carbopol and bioink properties, the printing parameters, and their close interactions, on the bioprinting fidelity have not been fully examined.[6,17,18] Thus, performing an in-depth quantitative analysis to determine optimal bioprint parameters to create hydrogel structures with adequate fidelity and consistency is prominent for embedded bioprinting.

In this work, we developed an experimental approach, verified by a theoretical method, to precisely control the fabrication process of soft hydrogel structures using 3D embedded bioprinting. Gelatin methacryloyl (gelMA), a modified photo-cross-linkable hydrogel which is derived by reacting methacrylic anhydride with gelatin, was used as the main hydrogel bioink for bioprinting.[19] By incorporation and control of photoinitiators, and using light irradiation (e.g., UV, blue light, white light), the groups of methacrylamide and methacrylate of gelatin chain can be polymerized to achieve a stable cross-linked hydrogel.[20] While gelMA-based hydrogels have been widely used in various tissue engineering and 3D biofabrication applications, the use of this versatile hydrogel bioink in 3D embedded bioprinting and the subsequent quantification of print fidelity have not been investigated. Here, we systematically examined the close interplay between the rheological properties of Carbopol solution and gelMA precursor, as well as printing parameters such as temperature, pressure, and volumetric flow rate. The mechanical properties of printed gelMA after UV cross-linking were also examined. Finally, we assessed the performance of human umbilical vein endothelial cells (HUVECs) after embedded bioprinting. This method can be used to generate reproducible and consistent tissue engineered constructs for use in a wide variety of applications, including in vitro disease modeling and drug screening, as well as in vivo regenerative therapies.

RESULTS AND DISCUSSION

While embedded bioprinting of photo-cross-linkable hydrogel bioinks has been previously studied,[14,15,21] the utilization of biocompatible gelMA-based hydrogels in these supported printing modalities has not been reported. There still seems to be a lack of systematic well-characterized workflows to conduct such bioprinting processes in a highly controlled manner, at a predefined fidelity and precision. In this study we utilized a hybrid approach, i.e., both experimental and theoretical tools, to enable in-depth characterization and optimization of embedded bioprinting processes using gelMA inks. We examined the efficacy of the developed platform in the high-fidelity manufacturing of a variety of 3D gelMA scaffold architectures, with or without cells, using Carbopol as suspension bath. Carbopol was selected as the support bath as it performs desired rheological behavior and provides a cell-friendly environment.[16] Also, compared to other existing methods, preparing Carbopol bath, extraction of the printouts, and the required post processing steps are rather simple and efficient.[15]

Prior to bioprinting, the degree of methacrylation of gelMA was exanimated by the ^{1}H nuclear magnetic resonance (NMR) spectra (Figure S1 of the Supporting Information, SI). The obtained signal at 5.5 ppm (the protons of methacrylate vinyl group of MA) and the reduced signal at 3.0 ppm (the protons of methylene of lysine) confirmed the efficient modification of gelatin by methacryloyl. By treating the aromatic amino acid moieties in gelatin as a reference, the degree of methacrylation was calculated at 88.86 ± 1.01% following eq 1.

The rheological behavior of bioinks has been proven to play a key role in determining the printing quality and consistency in extrusion-based bioprinting procedures.[22] Bioinks that exhibit viscous shear-thinning and that have loss modulus (G'') to storage modulus (G') ratios (i.e., loss tangent, G''/G') within a certain range would be preferred as candidate bioinks as they can provide self-support during the material deposition, while ensuring a fluent and uniform extrusion process without severe needle clogging.[23,24] In this work, we first evaluated the rheological behavior of gelMA bioinks by performing a temperature sweep on both 5 and 10% gelMA solutions (Figure 1A). Lower temperatures induced a more viscous gelMA with larger G' value, while moving to high temperatures produced a more liquid-like solution with increased G'' value (Figure 1A). The gelling/liquefying points were identified as 24 and 26 °C for 5% and 10% gelMA solutions, respectively. Previous studies reported that hydrogel-based bioinks with $G' > G''$ (lower loss tangent values) exhibited sufficient mechanical strength to provide structural self-support during the layer-by-layer stacking.[25] Such printing strategy, however, heavily relies on the properties of hydrogel itself, if no other support materials are used. This would require rigorous control on printing temperature to allow for a smooth uniform extrusion to generate a successfully printed structure. Such processes can be time-consuming and are often associated with low reproducibility, especially when working with lower concentrations of gelMA bioinks (e.g., 5% gelMA solution).[26] With support baths, such as Carbopol, the efficiency and reproducibility of gelMA printing

https://dx.doi.org/10.1021/acsami.0c15078
ACS Appl. Mater. Interfaces 2020, 12, 44563−44577

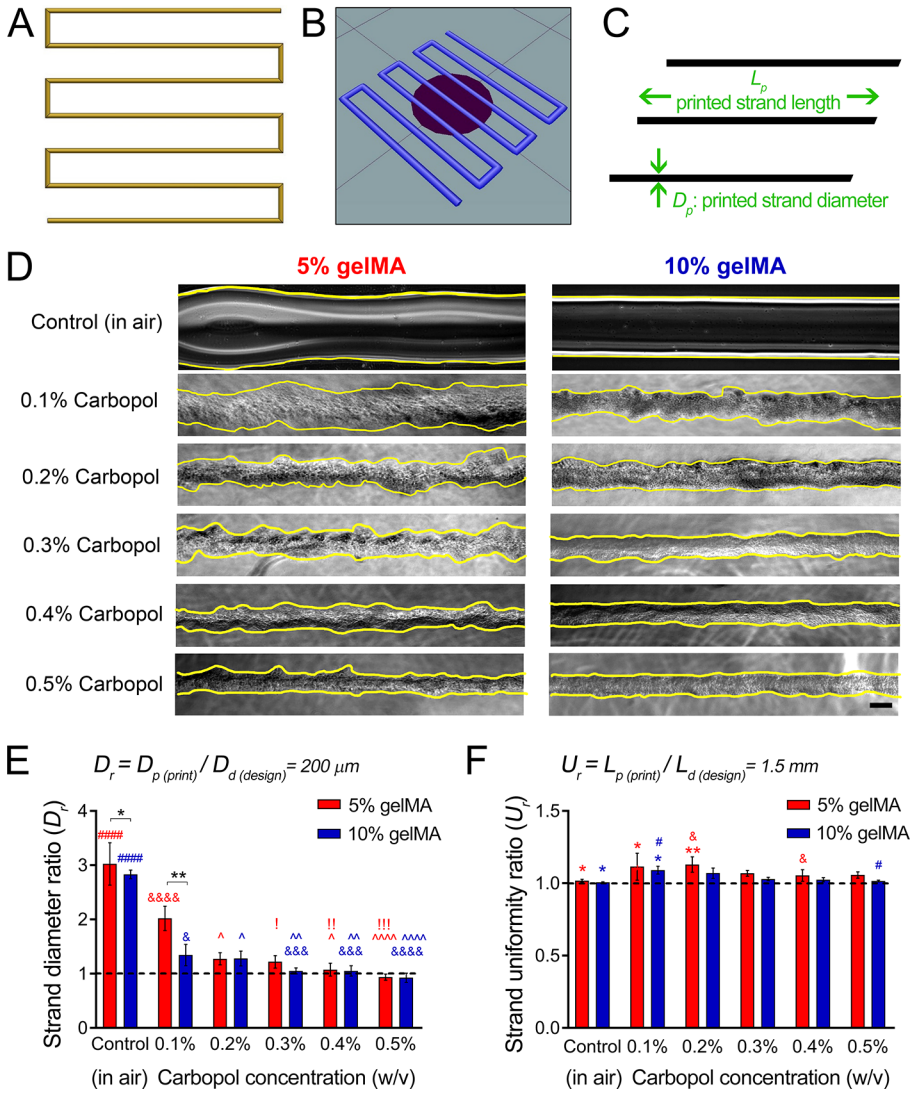

Figure 2. Characterization of printing fidelity of 5 and 10% gelMA bioinks in terms of *strand diameter ratio* ($D_r = D_p/D_d$) and *strand uniformity ratio* ($U_r = L_p/L_d$) parameters for 3D bioprinted single-layer structures. (A−C) Numerical (A) and g-code (B) models of single-layer construct used to assess fidelity by measuring printed strand diameter (D_p) and length (L_p) (C). (D) Bright field images of 5 and 10% gelMA strands, printed in the air (top row) and in Carbopol solutions with concentrations ranging from 0.1 to 0.5% (middle and bottom rows). (E) Quantification of the *strand diameter ratio*, D_r. (F) Quantification of the *strand uniformity* ratio, U_r. Scale bar represents 200 μm. One, two, three, and four symbols mean $p < 0.05$, 0.01, 0.001, and 0.0001, respectively.

can be significantly improved, since the structural integrity of the extruded gelMA would be preserved by Carbopol during the printing process, allowing for a wider range of usable printing parameters, such as speed and temperature.

On the basis of the obtained response of gelMA behavior to temperature changes, we selected 23 °C for the rest of bioprinting assays, where the G' values are greater than the G'' values for both gelMA bioinks (5 and 10% solutions).[25] Steady shear sweeps conducted at 23 °C showed that both gelMA ink formulations exhibited a non-Newtonian and shear thinning behavior (Figure 1B). As expected, a higher gelMA concentration showed a larger shear stress at a given shear rate, demonstrating a higher viscosity, thus requiring a higher printing pressure to reach a desired flow rate compared to the gelMA ink at a lower concentration.

The support bath in embedded bioprinting approach is designed to exert sufficient yield stress that can firmly hold the printed bioink after deposition, and meanwhile maintaining a shear thinning behavior, so it would not hinder the movement of the printing needle. Shear thinning behavior of Carbopol solutions with various concentrations ranging from 0.1 to 0.5% were selected as candidates to be used as a support bath (Figure 1C). Higher Carbopol concentration increased the viscosity of the solution. Under a given shear rate, the shear stress increased with the increase in Carbopol concentration. We next measured the yield stress by applying a range of small shear rates from 0.1 to 1 s^{-1} and interpolating the obtained shear stress values at zero shear rate based on a linear fitting (Figure 1D). The yield stress here ranged from 0.63 to 5.3 Pa, rising with the increase in Carbopol concentration. Time sweeps were also conducted on Carbopol solutions to assess the stability of Carbopol performance over time. Time-independent solution properties are typically preferred for support baths, as they are easy to maintain more consistent and predictable behavior during the printing process. Time sweeps for Carbopol showed a time-independent behavior of solutions under shearing at 23 °C, indicating its

https://dx.doi.org/10.1021/acsami.0c15078
ACS Appl. Mater. Interfaces 2020, 12, 44563−44577

stability within this time scale (Figure 1E). Another characteristic of an effective support bath is that it would allow for repeated retracing of the needle.[27] In short, it must be able to be fluidized locally when subjected to the stress around the moving printing needle, and then rapidly recover to solid state to firmly trap the extruded bioink. This time-dependent shear thinning and recovery behavior is also known as thixotropy.[28] Ideally, a solution with limited thixotropic time would be preferred as a support bath. In our study, the 0.1% Carbopol solution exhibited an evident thixotropic time, with large area between the hysteresis loop curves, while at Carbopol concentrations over 0.2%, the solutions performed limited thixotropic time with almost overlapped curves, indicating their ability to rapidly recover (Figure 1F).

As a preprinting step, we evaluated the injectability of gelMA solution, defined as the force needed for the activation of solution injection (Figure 1G,H). The force−displacement curves showed relatively stable dynamic glide forces for both 5 and 10% gelMA solutions, indicating that the prepared gelMA samples could be smoothly injected under relatively constant force (Figure 1H). The dynamic glide force for 10% gelMA sample was 16.7 ± 1.2 N, higher than that needed for the injection of 5% gelMA (4.4 ± 0.3 N). This difference could be mainly attributed to the rheological properties of gelMA solutions, where the 10% solution showed relatively higher flow viscosity compared to the 5% gelMA. It should be noted that the injectability of gelMA solution can be influenced by many factors such as the selected syringe, needle, as well as the compression speed. With a given experimental setup, gelMA at a higher concentration would always require a higher dynamic glide force to inject solution at a predefined flow rate.

It is well established that the printing process control markedly determines the shape of printed strands that act as the primary elements for the 3D structure assembly in extrusion-based bioprinting.[29−31] To that end, the first factor that we examined in for bioprinting process optimization was the volumetric flow rate of gelMA, which controlled the printing volume and therefore the size of printed strands. Flow rates can be affected by several parameters including printing pressure, needle diameter, and the behavior of bioink itself.[32] With constant needle gauge and bioink formulation, the flow rate is then mainly controlled by the printing pressure.[33] In this study, low printing pressures of 10 and 25 kPa were applied to extrude 5% and 10% gelMA bioinks, respectively, to obtain a constant flow rate of ∼0.33 μL/s for printing. These relatively low printing pressures were selected to avoid possible cellular damage when bioprinting cellular constructs. Printing pressure introduces process-induced mechanical forces when the ink is being extruded, to flow through the narrow needle, and these forces could cause injury to the cells.[34−37] With an identified flow rate, the critical printing speed was set accordingly, at 10 mm/s, leading to the printed strands with a diameter that theoretically matched with the inner diameter of the printing needle (200 μm) (based on eq 2).

Single-layer structures were printed in Carbopol solutions with concentrations ranging from 0.1% to 0.5% to assess the influence of support medium on printing fidelity in terms of strand diameter and uniformity (Figure 2). The diameter of printed strands was assessed by measuring the ratio of the actual diameter of printed strand (D_p) to the design diameter (D_d), i.e., *strand diameter ratio*, D_r (eq 3) (Figure 2A−C). The control group, made using conventional air printing (with no support), showed notable increase in the strand deformation and diameter in both 5% and 10% gelMA at 23 °C (Figure 2D,E). These could be attributed to the combined effects of the gelMA surface tension and the material self-consolidation (collapse) due to the gravity, as well as the extrusion swelling.[38,39] Owing to their relatively lower viscosity and storage modulus, printed 5% gelMA strands showed a larger deformation compared to the 10% gelMA, with a larger diameter ratio (D_r). When the Carbopol bath was employed, the deformation of printed strands was significantly reduced. The strand diameter decreased with the increase in Carbopol concentration (Figure 2D,E). This is likely attributed to the rheological behavior of Carbopol solutions as examined above where solutions with higher concentration exhibit larger yield stress (Figure 1D) and limited thixotropic time (Figure 1F), hence they are capable of more effectively retaining the strand geometry post extrusion. There was no significant difference observed in strand diameter when gelMA was printed in 0.4% versus 0.5% Carbopol bath, with diameter ratio (D_r) values approaching 1, indicating high printing fidelity (Figure 2E). Notably, D_r was smaller than 1 for gelMA printed in 0.5% Carbopol, indicating the actual diameter of printed strand was smaller than the calculated value. Such reduced strand diameter can be attributed to reduced flow rate of gelMA. Since the flow rate of gelMA was calculated based on the material deposition into air, it might be reduced due to the resistance of the support bath, especially when a more concentrated (0.5%) Carbopol solution is used under a constant printing pressure. This indicates that while increasing Carbopol concentration can be beneficial by providing a greater mechanical support for printed strands, there is an optimal range, beyond which increased Carbopol concentration would impede the printing flow and result in diminished bioprinted fidelity. On the basis of this *strand diameter ratio* analysis, a 0.4% Carbopol seems to provide optimal embedded bioprinting fidelity.

The uniformity of printed strands was also evaluated in single-layer prints by measuring the ratio of the actual length of printed strand (L_p) to the designed length (L_d), i.e., *strand uniformity ratio*, U_r (eq 4) (Figure 2C). Strands printed in the air showed uniform lines with U_r ratio close to 1 (yellow lines, Figure 2D). While strands printed in the Carbopol with concentrations less than 0.3% displayed obvious bumpy lines with significantly larger U_r values (Figure 2D,F). The acceptable uniformity of air printing can be attributed to the evenly distributed surface tension of gelMA bioink. The lower uniformity for Carbopol printing at low concentrations could be due to the gelMA infiltration through the gaps between Carbopol granular particles.[40] Additionally, the granular particles would influence the extruded lines and their surface depending on the grain size.[15] In this work, particle size was primarily smaller than 30 μm (Figure S2). At certain granular sizes, when fewer particles exist (i.e., lower Carbopol concentrations), printed strands, especially those at lower viscosity (e.g., 5% gelMA), could more readily diffuse into the larger gaps between granular particles. As more particles are added to the bath, the gaps will be occupied and this will significantly limit the infiltration, leading to more uniform extrusion lines (Figure 2D, bottom row). Therefore, for high-fidelity bioprinting of soft hydrogel bioinks, with low viscosities and high loss moduli, a support bath with a high material concentration and high granular particle numbers would be required. The U_r ratio did not significantly change when the Carbopol concentration was increased above 0.3%. Consistent with the *strand diameter* ratio analysis, we concluded

https://dx.doi.org/10.1021/acsami.0c15078
ACS Appl. Mater. Interfaces 2020, 12, 44563−44577

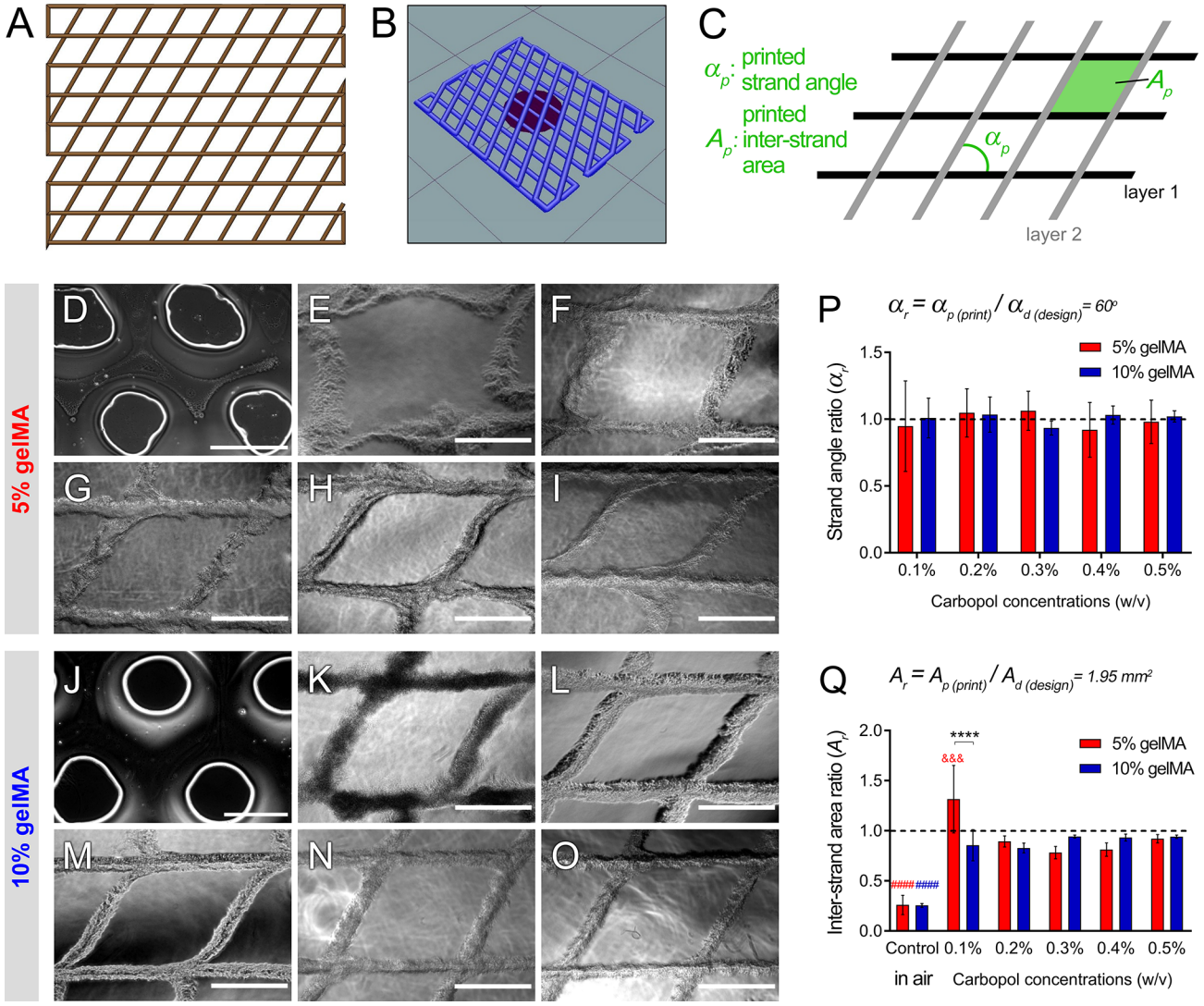

Figure 3. Characterization of printing fidelity of 5 and 10% gelMA bioinks 3D bioprinted two-layer structures. (A−C) Numerical (A) and g-code (B) models of single-layer construct used to assess fidelity by measuring printed strand angle (α_s) and interstrand area (A_s) (C). (D) Bright field image of 5% gelMA printed in the air as control. (E−I) Images of 5% gelMA printed in Carbopol with concentration of 0.1% (E), 0.2% (F), 0.3% (G), 0.4% (H), and 0.5% (I). (J) Bright field image of 10% gelMA printed in the air as control. (K−O) Images 10% gelMA printed in Carbopol with concentration of 0.1% (K), 0.2% (L), 0.3% (M), 0.4% (N), and 0.5% (O). (P−Q) Quantitative analysis of strand angle ratio, α_r, and interstrand area ratio, A_r based on the images in panels D−O. Scale bar represents 1 mm. Three and four symbols represent $p < 0.001$ and $p < 0.0001$, respectively.

that a 0.4% Carbopol solution is preferred for embedded bioprinting with both 5 and 10% gelMA bioinks.

Although gelMA-based bioinks with various concentrations have been printed in the air under rigorous temperature control, considerable deformation of extruded strands in these extrusion prints is almost inevitable, which can reduce the printing fidelity and introduce considerable changes in structural parameters (e.g., strand diameter, pore size, and construct bulk geometry).[25,41,42] To verify whether printing within a support bath could enhance the fidelity of gelMA scaffolds, we further compared the structural accuracy of bioprinted gelMA in air versus Carbopol (Figure 3). Printing fidelity was assessed for two-layer structures bioprinted within Carbopol solutions (or air) by quantifying *strand angle ratio*, α_r, and *interstrand area ratio*, A_r, between the strands of two layers (Figure 3A−C). In the control group, where gelMA was printed conventionally in the air, strand angles were hard to identify and measure, due to the gelMA ink spreading and layers fusion. Thereupon, the strand angle for the control group was not quantified. No significant difference was observed in the angles between strands printed in various Carbopol solutions (Figure 3D−P). However, compared to 10% gelMA, the 5% gelMA strands showed greater levels of variation in their angles (*strand angle ratio*, α_r), especially for those printed in lower concentrations of Carbopol (Figure 3P). The examination of *interstrand angle area*, A_r, showed a significant difference between the two-layer structures printed in 0.1% Carbopol −5% gelMA (Figure 3E) and other groups, indicating a major strands deformation, between the two layers, in that group. Such distortion in the area could be mainly due to the limited mechanical support of the low-concentration Carbopol bath and the less viscous gelMA bioink. During printing, the extruded gelMA strand was dragged from its designed position by the moving needle. This positional deviation of deposited strands led to the alteration of printed structural size as well as the pore area. Compared to the Carbopol groups, the interstrand area in air printed controls was

https://dx.doi.org/10.1021/acsami.0c15078
ACS Appl. Mater. Interfaces 2020, 12, 44563−44577

Table 1. Summary of Print Parameters Used in This Study for the Embedded Bioprinting of gelMA

GelMA concentration (gelMA)	Carbopol concentration (w/v)	print temp (°C)	needle gauge	printing flow rate	print speed (mm/s)	layer height (μm)
5%	0.4%	23	27 (0.5" in length, 200 μm in diameter)	~0.33 μL/s (can be adjusted based on applications)	10	200
10%	0.4%	23	27 (0.5" in length, 200 μm in diameter)	~0.33 μL/s (can be adjusted based on applications)	10	200

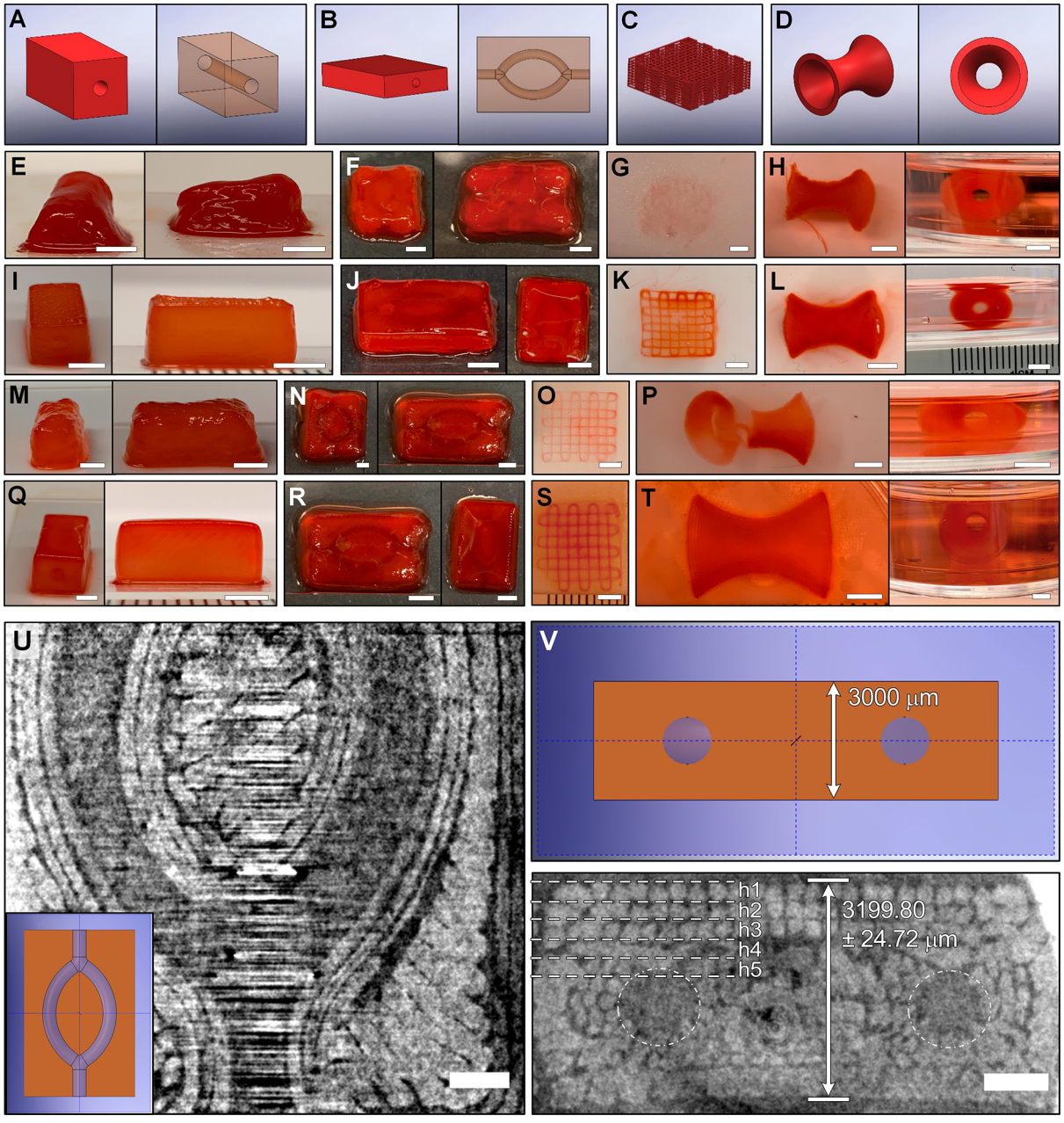

Figure 4. Embedded bioprinting of 3D complex structures using our established approach. (A–D) 3D structure CAD designs, including a hollow cube (A), a vessel model (B), a lattice scaffold (C), and a hollow drum (D). (E–H) 5% gelMA was printed in 0.1% Carbopol solution (as control) to create the hollow cubic (E), vessel (F), lattice (G), and hollow drum (H) constructs. (I–L) 5% gelMA was printed in 0.4% Carbopol solution to create the same constructs printed in E–H. (M–P) 10% gelMA was printed in 0.1% Carbopol solution as control to create the hollow cubic (M), vessel (N), lattice (O), and hollow drum (P) structures. (Q–T) 10% gelMA printed in 0.4% Carbopol solution. (U–V) Top (U) and side (V) views of the bioprinted vessel model, acquired by synchrotron radiation X-ray propagation-based imaging (PBI-CT) method, with the layer heights h1 to h5 equal to 247.91 ± 17.80, 241.38 ± 28.31, 243.27 ± 18.14, 246.57 ± 37.30, and 218.79 ± 26.03 μm, respectively. Scale bars in E to T represent 3 mm, and in U and V represent 1 mm.

significantly reduced and largely lost its designed shape due the strand deformation and fusion (Figure 3D,J).

On the basis of quantitative analysis of the four parameters discussed (D_r, U_r, α_r, and A_r), we picked a Carbopol solution with a 0.4% concentration as the support bath for the rest of

https://dx.doi.org/10.1021/acsami.0c15078
ACS Appl. Mater. Interfaces 2020, 12, 44563–44577

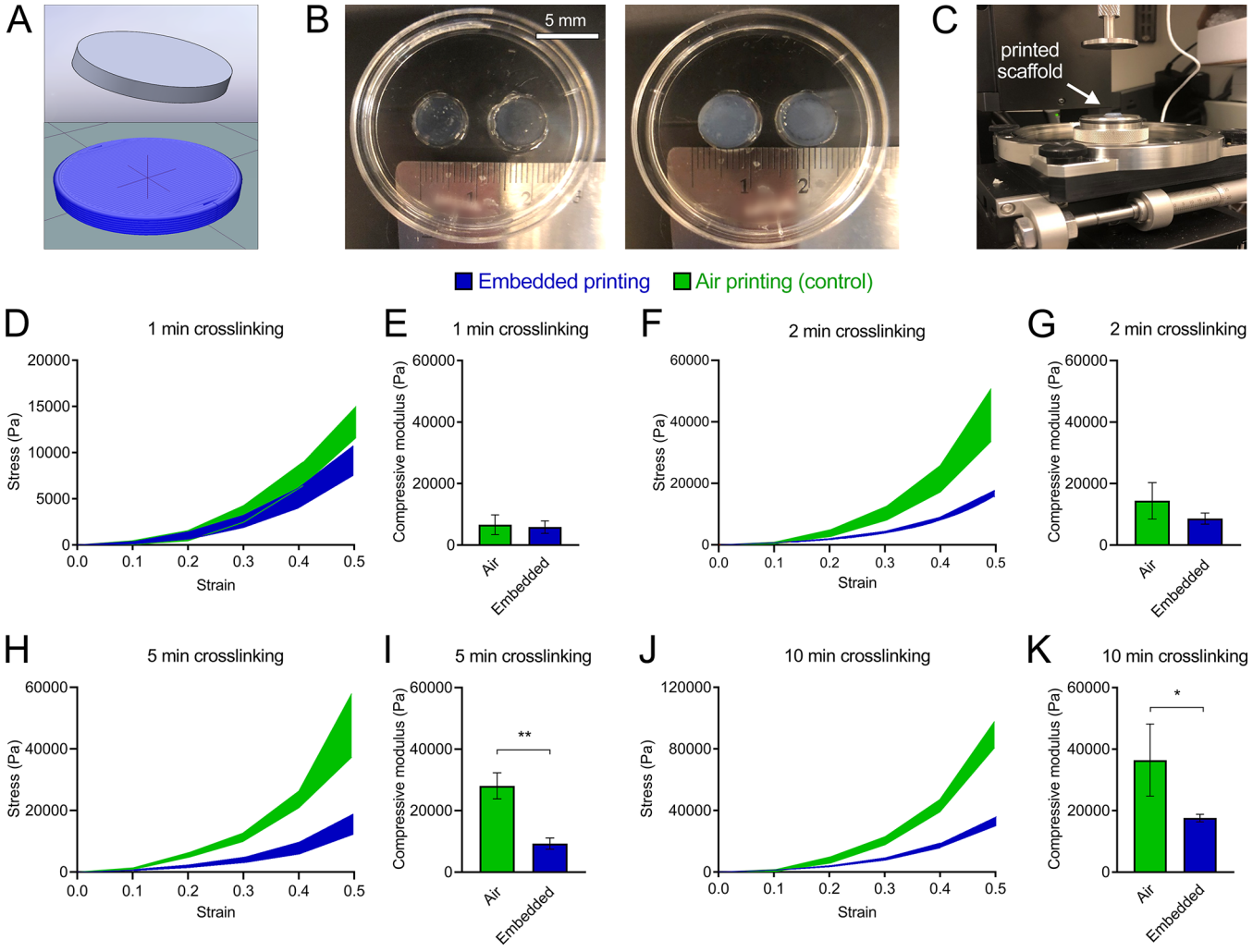

Figure 5. Influence of Carbopol solution (embedded bioprinting) on gelMA cross-linking under various UV exposure times, in comparison to the air printed control. (A) Designed CAD model for compression test (left) and the g-code (right) for 3D bioprinting. (B) Disc gelMA samples printed in air (left) and within Carbopol solution (right). (C) Unconfined compression testing setup used to assess compressive modulus of bioprinted scaffolds. (D–K) Stress–strain curves, up to 50% strain, obtained from sample compressions and corresponding compressive modulus measurement for gelMA constructs cross-linked for various UV exposure periods (constant UV intensity), including: 1 min (D–E), 2 min (F–G), 5 min (H–I), and 10 min (J–K). * represents $p < 0.05$ and ** represents $p < 0.01$.

embedded 3D bioprinting of gelMA structures (summarized printing parameters listed in Table 1). While previous works mainly focus on the adjustment of embedding bath or bioink types for the fidelity enhnancmenet,[15,18,40,43] here we demonstrated that the close interactions between the Carbopol bath properties, the gelMA rheological behavior, and the print process control can more effectively regulate the structure fidelity. In general, we recommend the use of high Carbopol concentrations to preserve high printing fidelity, especially when low-viscosity hydrogel bioinks are used. Following the printing conditions, we next bioprinted four 3D models using the optimized embedded printing conditions: (1) a hollow cube (Figure 4A), (2) a vessel model (Figure 4B), (3) a lattice scaffold (Figure 4C), and (4) a hollow drum (Figure 4D). The 0.1% Carbopol printing was used as control. GelMA constructs printing within the 0.4% Carbopol well represented the designed geometries with relatively clear and sharp edges and surfaces, while evident structural deformation was observed in constructs printed in 0.1% Carbopol (Figure 4E–T, Figure S3, and SI Movies S1 and S2). These results demonstrate the efficacy of the developed embedded printing method to create complex 3D structures with adequate structural fidelity.

While there has been increasing interest in bioprinting a variety of gelMA based bioinks, little progress has been made in noninvasive assessment of the resolution of bioprinted constructs. Visualization of the 3D thick gelMA constructs using conventional imaging techniques has been hampered due to the relatively low density and weak X-ray attenuation of these hydrogels.[44] The laboratory-scale X-ray CT techniques show limited ability to visualize weakly absorbing materials, such as hydrogels. To achieve adequate X-ray attenuation, for CT imaging, printed hydrogel structures require additional post processing, which may be damaging to the structure.[44] Alternatively, magnetic resonance imaging (MRI) and ultrasound imaging (UI) are used for soft tissue visualization.[45,46] However, both techniques face constraints to achieve high spatial resolutions (micrometer level) within feasible scan times.[47] The X-ray propagation-based imaging (PBI) technique, which introduces X-ray refraction signal to predictions, has shown promise in the visualization of low-density materials due to the much larger refractive index variations, compared to the

https://dx.doi.org/10.1021/acsami.0c15078
ACS Appl. Mater. Interfaces 2020, 12, 44563–44577

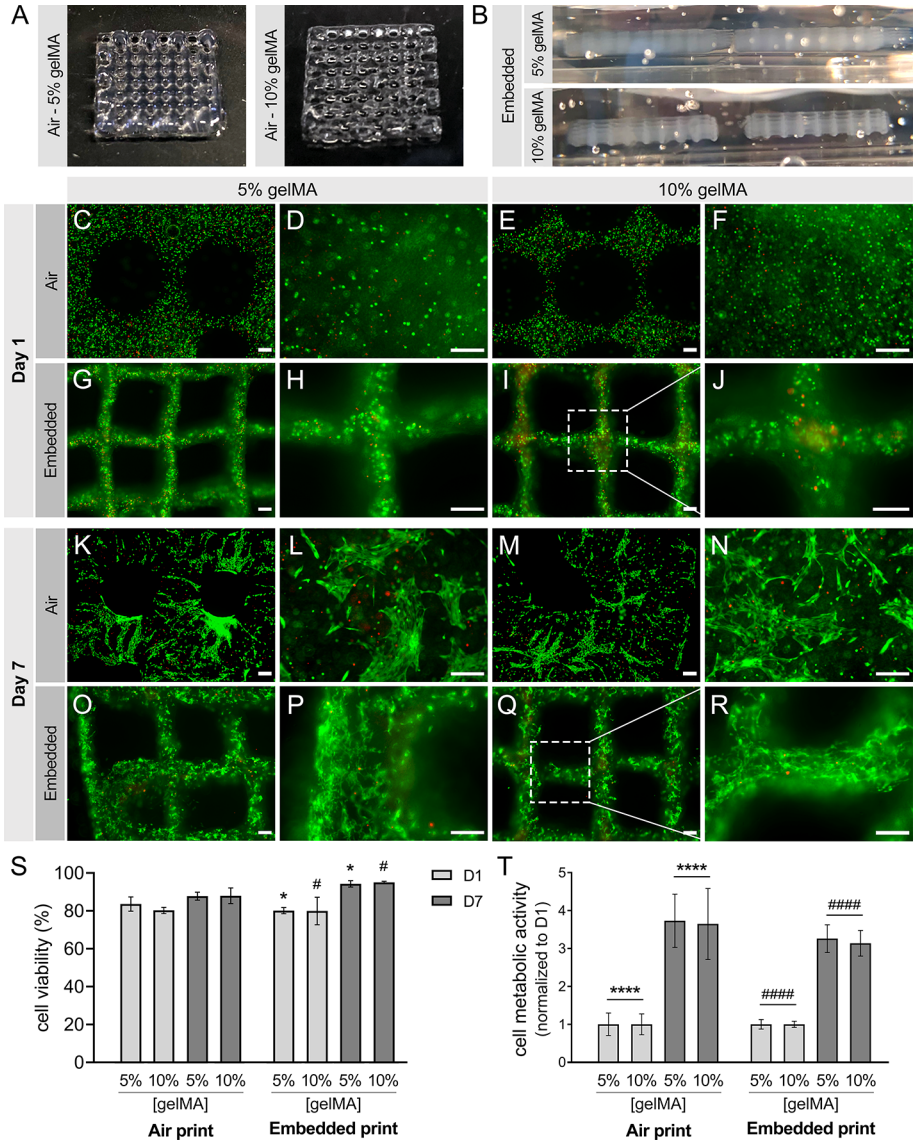

Figure 6. Embedded cellular bioprinting using the optimized print process identified in this study. (A) Air printed scaffold using 5% (left) and 10% gelMA (right). (B) Embedded printed scaffold using 5% (top) and 10% gelMA (bottom). (C–J) Live/Dead assay results from day 1, performed on air printed scaffold with 5% (C,D) and 10% gelMA (E,F), and embedded printed scaffold with 5% (G,H) and 10% gelMA (I,J). (K–R) Live/Dead results from day 7, for air printed scaffold with 5% (K,L) and 10% gelMA (M,N), and embedded printed with 5% (O,P) and 10% gelMA (Q,R). (S) Quantitative analysis of cell viability based on the Live/Dead results. (T) AlamarBlue assay on HUVECs encapsulated in bioprinted scaffolds. Scale bars in A and B represent 10 mm, and in C through R represent 200 μm. * and # in S represent the statistical difference between 5% and 10% gelMA samples, respectively, with $p < 0.05$. **** and #### in T represent the statistical difference between day 1 and day 7 for air and embedded bioprinted samples, respectively, with $p < 0.0001$.

variations in X-ray absorption coefficient. In combination with a synchrotron radiation that is highly brilliant and coherent light source, such a technique has shown great capacity in visualizing soft tissues without the need of additional treatment.[47] In this work, the SR-PBI-CT method was applied to characterize the structural details of embedded printed gelMA scaffolds. It was further used to quantify the printing fidelity of the vessel model described above (Figure 4B). Synchrotron imaging captured the details of the printed strands and their patterns, as well as the vessel channels that were formed by the strands (Figure 4U–V, SI Movies S3). The top view shows the relatively uniform boundaries of printed hollow vessel channels with the measured diameter of 1.24 ± 0.12 mm, which well corresponds to the design diameter (1.2 mm). The side view image further demonstrates uniform and parallel distribution patterns of printed strands and their correspondence to the designed model, with the total structural height of 3.20 ± 0.02 mm and layer height of less than 250 μm after measuring the top 5 layers, which closely match the designed model (3 mm in height) and the slicing layer height from GCode (Figure 4V). Microscale porosity (smaller than 50 μm) between adjacent strands can be attributed to the inherent nature of the layer-by-layer bioprinting method and the robust support provided by the Carbopol bath, resulting in limited material fusions between individual strands (Figure 4V, bottom). The decreased quantity and size of micropores from top to the bottom of construct, may be attributed to the partial consolidation of soft, mechanically unstable hydrogel due to the gravity (so-called self-compression[48−50]).

https://dx.doi.org/10.1021/acsami.0c15078
ACS Appl. Mater. Interfaces 2020, 12, 44563−44577

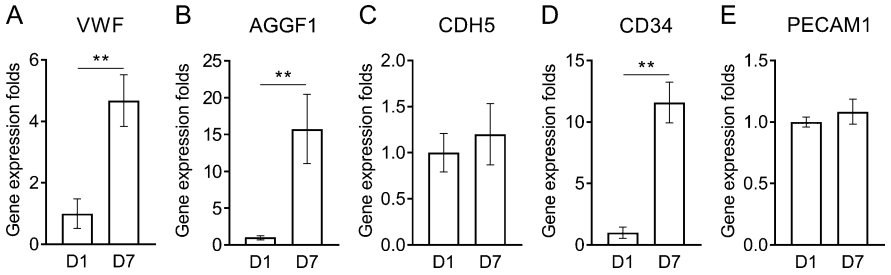

Figure 7. Gene expression of HUVECs in embedded bioprinted gelMA constructs, including (A) VWF, (B) AGGF1, (C) CDH5, (D) CD34, and (E) PECAM1. ** indicates $p < 0.01$.

Manipulation and tuning mechanical properties of bioprinted hydrogel constructs, such as stiffness, are increasingly used as a way to exert essential impacts not only on the structural integrity, but also on the biological functions of living cells.[51,52] It is known that the intensity and duration of ultraviolet (UV) light cross-linking plays a key role in tailoring the mechanical stiffness of gelMA-based hydrogels—higher UV light intensity and/or longer exposure time results in a stiffer gelMA substrate.[19] For most embedded bioprinting systems, UV light can readily penetrate the Carbopol solution and reach to the printed gelMA structure for curing. However, the intensity of UV light could be attenuated during penetration, resulting in reduced, nonuniform stiffness of gelMA constructs.[20] Such impacts have not been explored experimentally. Here, we printed 10% gelMA structures in air (control) and in 0.4% Carbopol solution, and measured the hydrogel stiffness, obtained by tuning the UV exposure period (Figure 5A−C). The control was printed under temperature control to preserve its self-support. The size difference between these two groups was minor and such difference would not affect the compressive modulus measurement as the modulus reflected the properties of the gelMA. The compressive modulus of gelMA scaffolds printed in air varied from 6.6 ± 2.7 kPa to 36.4 ± 10.2 kPa, while the values of Carbopol printed gelMA ranged from 5.9 ± 1.8 kPa to 17.6 ± 1.1 kPa (Figure 5D−K). Expectedly, the gelMA stiffness increased with the extension of UV exposure time. Of note, construct stiffness decreased when cured within the Carbopol bath, compared to the control samples that were printed and cured in air. This difference became significant at UV exposure times over 5 min (Figure 5H−K). This demonstrated the impact of Carbopol support bath to hinder the UV light penetration. These findings would provide more precise guidance to design and tune mechanical properties of a broad range of photopolymerizable constructs that are fabricated via embedded bioprinting. While we only tested one Carbopol bath concentration (0.4%), we speculate that the concentration of support bath may play an important role in alteration of the UV absorption (penetration), thus impacting the mechanical stiffness of the cured hydrogel constructs.

The support bath in 3D embedded bioprinting is required also to offer a biocompatible environment for living cells when they are incorporated in the biofabrication processes.[40] To investigate the cytocompatibility of the Carbopol solution used in this study, HUVECs were encapsulated in gelMA and bioprinted into 10-layer lattice scaffolds in Carbopol. Cell viability and growth were evaluated for 7 days (Figure 6). Control groups were prepared by bioprinting HUVEC/gelMA in the air (Figure 6A,B). Both air and embedded bioprinted samples demonstrated a high cell viability which was over 78% a week after the bioprinting (Figure 6C−S, Table S1). The difference between the control and embedded bioprinted samples was limited with no significance. Similarly, the noninvasive AlamarBlue assay demonstrated the proliferative capability of HUVECs in gelMA constructs, showing no significant difference between air and Carbopol bioprinting, with a ∼3-fold growth rate after 7 days (Figure 6T). The relatively larger variation in the metabolic activity readouts of air printed samples, compared to those printed using embedded method, may be due to the limited printing consistency in the air. Of note, by day 7, HUVECs exhibited an elongated morphology and a preferred orientation, indicating adequate cellular compatibility and affinity with the extruded strands (Figure 6K−R). Results from qPCR showed significant increase of EC-specific genes expression, including VWF, AGGF1, and CD34 at day 7 compared to day 1. The increased expression levels of von Willebrand factor, angiogenic factor, and adhesion molecule, suggest enhanced function of HUVECs encapsulated in gelMA after embedded bioprinting (Figure 7, Table S2). Meanwhile, the CDH5 and PECAM1 expression levels were relatively stable, with some insignificant increases on day 7 compared to day 1. All these results confirmed the cytocompatibility of the used Carbopol solution, demonstrating its potential to be used as a support bath in various embedded bioprinting endeavors.[15,16] The observed cell death (∼20%) could be attributed to the printing process-induced mechanical stresses such as shear stress and extensional stress, as well as the osmotic pressure.[53] To further enhance cell support, one anticipated strategy is to minimize these mechanical stresses by reducing printing pressure, or using different printing needle types such as tapered needles which can lower process-induced shear stress.[37,54] Another strategy is to prepare Carbopol solutions using culture media as solvent, which can provide a more balanced cell osmotic environment.[35]

In summary, this study demonstrated that a well-characterized and optimized embedded bioprinting approach, with extensive printing process controls, greatly improves fabrication of soft hydrogel structures with high printing fidelity, while maintaining acceptable cell viability and functions. One major concern for gelMA bioprinting with functional cells is the utilization of UV light, which could introduce cellular damage during the cross-linking process and therefore impact the subsequent (especially, in vivo) applications of such bioprinted constructs.[26] While alternative bioink curing methods, such as visible light or chemical cross-linking methods, have been developed, their relatively slow and less characterized curing processes may introduce issues for forming 3D constructs with high structural integrity and fidelity.[55] Embedded bioprinting enables utilization of these alternative, slower, and more cell-friendly curing methods by maintaining the printing fidelity of gelMA, or other soft hydrogel bioinks, during the cross-linking process.

https://dx.doi.org/10.1021/acsami.0c15078
ACS Appl. Mater. Interfaces 2020, 12, 44563−44577

CONCLUSIONS

3D bioprinting of hydrogel-based constructs has shown great promise in biomedical engineering applications, yet still faces a substantial challenge to ensure consistent printing fidelity. Our work establishes a new, well characterized workflow for creating hydrogel structures with desired fidelity based on embedded bioprinting techniques. Our theoretical discussion, coupled with experimental results, demonstrates the significance of printing flow rate of gelMA bioink (or other soft hydrogels), which can be adjusted through tuning the temperature, needle size, and printing pressure, according to the rheological behavior of the biopolymer. The concentration of Carbopol dictated its rheological behavior, and the 0.4% Carbopol solution was observed to be optimal, as it robustly preserved the printed structures with high fidelity, while not disturbing or blocking the print flow of the gelMA bioink. Using this optimized configuration, a variety of 3D structures with intricate inner hollow structures were reproducibly bioprinted and non-invasively visualized using the novel SR-PBI-CT method. Further, for the first time, we reported on the influence of the Carbopol bath on UV penetration, and consequently, the stiffness of embedded printed constructs. It was shown that the Carbopol bath could present a hindrance against the UV light penetration, resulting in diminished mechanical properties of printed hydrogels, an important factor to consider in future scaffold design and manufacturing endeavors. This study demonstrates the significant role that close interplay between rheological behavior of hydrogel bioinks, support medium, and printing parameters can have on the embedded 3D bioprinting process. Results from this study will help establish a robust platform for the design and manufacture of varied hydrogel scaffold systems, with minimal amount of trial-and-error, to achieve optimal print fidelity and cell support.

MATERIALS AND METHODS

Materials. Gelatin from porcine skin (Type A, SLCC7838), methacrylic anhydride (MA), Irgacure (2-Hydroxy-4′-(2-hydroxyethoxy)-2-methylpropiophenone), and PBS were purchased from Sigma-Aldrich (Wisconsin, U.S.A.). Carbopol ETD 2020 polymer was purchased from Lubrizol (Wickliffe, U.S.A.). Calcein AM and propidium iodide (PI) were obtained from Biotium (Fremont, U.S.A.). Cell culture medium (VascuLife VEGF) was purchased from Lifeline Cell Technology (Oceanside, U.S.A.).

GelMA and Carbopol Solution Preparation. GelMA was synthesized following the protocol described previously.[56] Briefly, a 5 g gelatin was mixed at 10% (w/v) into PBS at 50 °C until fully dissolved. A 4 mL MA was then added for gelatin modification at 50 °C for 3 h. Following a dilution with additional warm PBS to stop the reaction for 15 min, the mixture was dialyzed against Milli-Q water using dialysis bags for 1 week at 40 °C to remove salts and methacrylic acid (with water change 2−3 times a day). The solution was then lyophilized (for 5−7 days) and stored away from light at −20 °C until use. GelMA solutions with concentrations of 5% and 10% w/v were prepared by reconstituting lyophilized gelMA powder into sterilized PBS with 0.5% w/v Irgacure. GelMA solutions were stored away from ambient light at 4 °C for no longer than 2 weeks.

Carbopol powder was gradually added into Milli-Q water with a concentration of 0.5% w/v and stirred at a speed over 800 rpm at room temperature for 24 h. The suspended Carbopol was aliquoted into 50 mL centrifuge tubes and diluted by Milli-Q water to achieve Carbopol media with concentrations ranging from 0.1 to 0.5%. The pH balance was performed by adding 4 M NaOH with certain amounts. The balanced Carbopol medium in the tubes were centrifuged at 3500 rpm for 10 min for degassing, and later stored at 4 °C for printing. For cell printing, Carbopol powder was first sterilized by UV exposure for 40 min and then dissolved following the same procedure under sterile conditions.

GelMA Characterization. The degree of methacrylation of gelMA was quantified using ^{1}H NMR at the Emory University NMR center according to previously method.[57] Briefly, a 10 mg lyophilized gelMA or gelatin powder was dissolved in 7.5 mL in deuterium oxide at 37 °C for 1 h. After evaluation, the peak area of aromatic acids in the samples of both gelMA and gelatin was employed as a reference in each spectrum. The peak area of lysine methylene protons showing around 3.0 ppm was sued for calculation of the degree of methacrylation (DM):

$$\mathrm{DM} = \left(1 - \frac{\text{area of lysine methylene of gelMA}}{\text{area of lysine methylene of gelatin}}\right) \times 100\% \quad (1)$$

GelMA from three different batches were collected and examined (n = 3), with the average values expressed for analysis.

Assessment of Rheological Properties of gelMA and Carbopol Solutions. Rheological properties of gelMA and Carbopol with various concentrations were assessed using an AR-G2 rheometer (TA Instruments, U.S.A.). For gelMA, 800 μL of the solution was loaded into the gap between parallel upper and lower plates of the rheometer (25 mm in diameter, 400 μm gap). Any extra solution that was squeezed out was removed by a scraper. A temperature sweep from 30 to 5 °C was conducted at a rate of −1 °C per 60 s. The influences of temperature on the storage moduli, G', and loss moduli, G'', for both 5% and 10% gelMA were recorded at a constant frequency (1 Hz) and strain amplitude (1%). A steady shear sweep ranging from 1 to 2000 s^{-1} at 23 °C was then performed to measure the flow behavior of gelMA solutions. For Carbopol, a time sweep and a steady shear sweep were conducted on Carbopol solutions. A 20 min time sweep was performed at 23 °C to measure the response of Carbopol solution as a function of time. The steady shear at shear rates ranging from 0.01 to 1000 s^{-1} was performed to identify the flow pattern as well as the yield stress of Carbopol solution. Thixotropy was also evaluated on Carbopol solutions based on the hysteresis loops which were obtained from increasing and decreasing shear on Carbopol, with controlled shear stress from 0 to 100 Pa. Each of the tests were repeated three times (n = 3).

Assessment of GelMA Injectability. The measurement of the injection force was performed in a compression model using a Mach-1 mechanical testing machine (Biomomentum Inc., Canada). GelMA solutions in 5% and 10% concentrations were separately pipetted into a 5 mL syringe (gelMA volume of 1 mL). The syringe was connected to a gauge 27 needle with a needle length of 0.5". After stabilizing at room temperature for 20 min, gelMA solution was ejected by pushing the plunger of the syringe at a speed of 0.2 mm/s for injection (using the Mach-1 compressive device) until the entire volume of gelMA was ejected. The force−displacement curve was recorded via Mach-1. The injection for each gelMA concentration was repeated three times (n = 3) and the average values were used for analysis.

3D Printing Setup and Process Control for the Single and Two-Layer Constructs Manufacturing. For both single and two-layer structures, the designed strands were in cylindrical shapes, at a diameter of D_d = 200 μm. The distance between adjacent strands (length of strand) was L_d = 15 mm. The angle between the first and the second layer was designed at α_d = 60°. To start printing, 5% and 10% gelMA solutions were separately loaded into printing syringes of the BioX printer (CELLINK, U.S.A.). We first measured the volumetric flow rate of gelMA solution. Printing needle of 27 Gauge (200 μm in inner diameter) with a 0.5' needle length was selected for all of the prints. GelMA solutions were precooled for 20 min at a controlled temperature of 23 °C, and then were printed with a controlled printing pressure of either 10 or 25 kPa, to ensure a relatively consistent flow rate for 5% and 10% gelMA, respectively. The printed solution within a certain period was weighed by a digital scale with a resolution of 0.01 mg, and the volumetric flow rate was then calculated given the gelMA solution density of 1 g/mL.

With a given flow rate, the shape of printed strands will be dominated by the control of printing speed.[58] Supposing that the flow rate of printed gelMA is Q, and that the deformation introduced by material

https://dx.doi.org/10.1021/acsami.0c15078
ACS Appl. Mater. Interfaces 2020, 12, 44563−44577

swelling or spreading can be ignored, the diameter of the printed strand (D_p) can be predicted by the following:[37]

$$D_p = \sqrt{\frac{4Q}{\pi V_p}} \quad (2)$$

where V_p is the printing speed. Thus, printing speed inversely influences the diameter of printed strand, and when the printed speed reaches a critical value, the diameter of strand will theoretically be equal to the inner diameter of the needle ($D_p = D_n$).

On the basis of the eq 2, a critical printing speed of 10 mm/s was calculated for our gelMA bioink, according to the flow rate measurements. The quality of printed structure will be not only determined by the control of flow rate and printing speed, but also significantly affected by the interaction between bioink and the support bath. To examine this latter effect and find out the optimal support bath, Carbopol solutions with varied concentrations, from 0.1 to 0.5%, were prepared as printing bath. Tested CAD models included one- and two-layer structures, with each layer consisting of multiple parallel contiguous lines (snake shape) (Figures 2A−C and 3A−C). Numerical structures were designed with SolidWorks 2018 (Dassault Systèmes, France) and were converted into G-code by Repetier (Figure S1C,D, Hot-world GmbH & Co. KG, Germany). Immediately after printing, the hydrogel structures were cross-linked under UV light with controlled intensity of 3.5 mW/cm^2 for 2 min and were examined under an optical microscope connected with a camera (Leica Microsystems DFC7000T, Germany).

Printing Fidelity Characterization. Optical microscopy images were acquired to assess printing fidelity using ImageJ (National Institutes of Health, Maryland USA). For this purpose, we quantified four geometrical factors, including: *strand diameter ratio*, *strand uniformity ratio*, *strand angle ratio*, and *interstrand area ratio*.

A *strand diameter ratio*, D_r, was defined as the ratio of the diameter of the actual printed strand (D_p) and the designed (CAD) diameter of strand (D_d = 200 μm):

$$D_r = \frac{\text{diameter of printed strand, } D_p}{\text{diameter of designed strand, } D_d} \quad (3)$$

The D_r parameter can be used to assess deformation of printed strands in the radial direction. A high printing fidelity is achieved when D_r values are equal or close to 1, while significant strand distortion exists when these ratio values are far from 1.

A *strand uniformity ratio*, U_r, was defined to measure the uniformity and consistency of the printed strands. To calculate U_r, the actual length of a printed strand (L_p), measured using optical microscopy images, was divided by the length of a perfectly uniform strand (i.e., a straight line) as designed (L_d = 1.5 mm):

$$U_r = \frac{\text{length of printed strand, } L_p}{\text{length of designed strand, } L_d = 1.5 \text{ mm}} \quad (4)$$

A nonuniform strand can be identified when U_r values are much greater than 1, while a uniform print is associated with U_r values close or equal to 1.

A *strand angle ratio* (α_r) was used to quantify the misplacement/distortion of printed layers (across two consecutive printed layers, Figure 3C). The following equation was used to calculate α_r:

$$\alpha_r = \frac{\text{actual angle between two printed strands, } \alpha_p}{\text{designed angle between two strands, } \alpha_d = 60^\circ} \quad (5)$$

As such, α_r values can illustrate a high printing fidelity with no layer misplacement when $\alpha_r \approx 1$, and a low structural fidelity when $\alpha_r > 1$ or $\alpha_r < 1$.

An interstrand area ratio, Ar, was defined to quantify the surface area of the quadrilateral openings created by four strands from two consecutive printed layers (Figure 3C). This parameter will therefore report on the variation of both strand uniformity and strand angle. Ar was determined by dividing the surface area of the actual printed quadrilateral opening (A_p) to that of the designed CAD model (A_d = 1.95 mm^2):

$$A_r = \frac{\text{actual surface area between printed strands, } A_p}{\text{designed surface area between strands, } A_d = 1.95 \text{ mm}^2} \quad (6)$$

Therefore, A_r values close to 1 will indicate relatively higher fidelity and as they diverge from 1, print fidelity deteriorates ($A_r > 1$ and $A_r < 1$).

Each 3D bioprinting test was repeated five times for both single- and two-layer structures, and three bright field microscopy images were acquired (randomly) from each construct and were manually measured (n = 15). Results from the fidelity analysis were used to identify the appropriate (i.e., optimal) Carbopol solution for gelMA fabrication and the rest of the study. Structures 3D printed without Carbopol supports (printed in air) were used as control.

Embedded Bioprinting of Complex 3D Structures−Bioprint Characterization Using Synchrotron Propagation-Based CT Imaging Technique. A variety of complex geometries were selected and embedded printed using the optimal conditions obtained above, to achieve maximal fidelity. GelMA constructs were bioprinted in a 0.4% Carbopol support bath. Printed structures were immediately cross-linked by UV light with (3.5 mW/cm^2 for 6 min). Subsequently, scaffolds were recovered from the Carbopol bath and washed in PBS three time for total 1 h on a rocker at room temperature (23 °C). Food dye was used to stain the structure for imaging. The same designs were also created within 0.1% Carbopol as a control group.

The prints were visualized using a recently developed, synchrotron radiation-based, propagation-based imaging (PBI) − CT technique (SR-PBI-CT).[2] This advanced imaging method was performed at the 05ID-2 beamline at the Biomedical Imaging and Therapy facility (BMIT), at the Canadian Light Source (CLS). A highly collimated monochromatic X-ray beam was generated. Samples were scanned at 30 keV. The Sample-to-Detector Distance (SDD) was set at 2 m. The detector was a beam monitor AA-60 (Hamamatsu Photonics, Shizuoka, Japan), coupled with an ORCA Flash 4.0 camera (Hamamatsu Photonics, Shizuoka, Japan) with the pixel size of 13.1 × 13.1 μm^2. The imaging field of view was set to 27 × 8.8 mm2. A total of 1800 projections over 180 °C were acquired per scan with the exposure time of 100 ms per projection. Phase retrieval was applied to convert edge enhancement phase contrast to areal contrast for further quantitative analysis. An open-source package—the Ultra-Fast-Online (UFO)—[59]was used to perform Paganin/TIE phase-retrieval[60] on the projections and was followed by CT reconstruction.

Assessment of Mechanical Properties of Printed gelMA Constructs in Carbopol Bath. Cylindrical samples, which have been extensively selected for the compression evaluation of hydrogels, were printed in Carbopol bath and also in the air (control) with temperature control with a diameter of 10 mm and a height of 1.5 mm.[61,62] A 0.4% Carbopol suspension was used as it preserves the structural fidelity of gelMA during printing. Printed samples were then cross-linked under UV light for 1, 2, 5, or 10 min, with a constant UV intensity of 3.5 mW/cm^2. Polymerized samples were transferred onto the platform of a Mach-1 mechanical testing machine for unconfined compression testing. The compression speed was set at 0.1 mm/s and the maximum moving distance was 50% of sample height. The compressive modulus for each sample was calculated from the linear section of the stress−strain curve (first 20% strain) and was obtained from the average value of four compressive tests (n = 4).

Cellular gelMA Bioprinting−3D Cell Culture. HUVECs (purchased from ATCC, U.S.A.) were cultured in tissue culture flasks in a humidified tissue culture incubator (37 °C with a 5% CO_2). Media (VascuLife VEGF Endothelial Medium Complete Kit) was used for HUVEC culture. A cell passage number of 17was used for all 3D bioprinting assays. After harvesting, cells were mixed with 10% gelMA at a density of 1 × 10^7 cells/mL. Subsequently, 10-layer cellular scaffolds in the form of a lattice structure (Figure 6) were bioprinted in a sterile environment, using the optimal printing process obtained above, using a 0.4% Carbopol solution as support bath. After cross-linking for 2 min at a UV intensity of 3.5 mW/cm^2, cell laden scaffolds were extracted from the bath and washed twice by PBS buffer (10 min each) on a rocker at room temperature. Then samples were transferred and

https://dx.doi.org/10.1021/acsami.0c15078
ACS Appl. Mater. Interfaces 2020, 12, 44563−44577

washed twice on a rocker using LifeFactors culture media at 37 °C for 1 h. Samples were then removed into a new plate for culture in the incubator. The final scaffolds were cultured in the incubator for desired times.

Cell Viability and Proliferation Assay. Cell viability in bioprinted 5% and 10% gelMA constructs was measured at days 1 and 7 post printing. Fluorescent dyes, calcein-AM with a final concentration of 1 μg/mL and PI with a final concentration of 20 μg/mL, which selectively stain live or dead cells, were added to the scaffold culture medium. After 30 min of incubation, scaffolds were washed with fresh culture medium for 5 min and observed with a fluorescence microscope (Leica Microsystems). At each time point, three images were randomly taken and subsequently analyzed using ImageJ. GelMA samples that were fabricated in air by temperature control were used as control.

Cell proliferation was assessed using AlamarBlue assay.[48,63,64] Briefly, the AlamarBlue reagent (Bio-Rad, U.S.A.) was added to fresh HUVEC culture medium in a 1:9 volumetric ratio and added to the wells in culture plates containing the printed scaffolds and incubated for 5 h. Next, 100 μL of the media was collected from each well, placed in a 96-well plate, and the absorbance was read using a microplate reader (BioTek Instruments, U.S.A.) at the wavelengths of 550 and 600 nm. Values were obtained on days 1 and 7 and were normalized by the day 1 as baseline. Four scaffolds were printed for this assay (n = 4).

Gene Expression. Quantitative real-time PCR assay was used to characterize the gene expression of HUVECs after embedded bioprinting. Printed hydrogel scaffolds (10% gelMA) was first digested by collagenase dissolved in PBS at 4 mg/mL, for 1 h in the incubator. The digested solution was collected and centrifuged at 800 rpm for 5 min. The supernatant was collected for RNA extraction using Trizol reagent (Bio-Rad). RNA was reverse-transcribed, and cDNA was synthesized using a SuperScript VILO cDNA Synthesis Kit (Thermofisher). qPCR was performed using a SYBR Green PCR master kit (Bio-Rad) and using a 7500 real time PCR system (Applied Biosystems). The relative gene expression was calculated using the $2^{-\Delta\Delta Ct}$ method with normalization to the Ct of the housekeeping gen GAPDH (Glyceraldehyde 3-phosphate dehydrogenase). Table S2 shows the primer sequences used for this study (Integrated DNA Technologies). Gene expression was assessed at days 1 and 7 post bioprinting. The values collected at day 1 were used to normalize data and obtain fold changes. Three samples were prepared at each time point (n = 3).

Statistical Analysis. Experimental data were calculated and expressed using mean values ± standard deviation (SD). Statistical significance was determined by ordinary one-way or two-way analysis of variance, and multiple comparisons were performed using t test and GraphPad Prism with an acceptable significance level of $p < 0.05$.

■ ASSOCIATED CONTENT

Supporting Information

The Supporting Information is available free of charge at https://pubs.acs.org/doi/10.1021/acsami.0c15078.

Degree of methacrylation of gelMA, size of Carbopol microparticles, models and inner structure after sectioning, live and dead cell numbers, HUVECs primer, hollow cubic structure with open lumen, vessel model with open lumen, and visualization of 3D printed vessel model (PDF)

Structural deformation in constructs printed in 0.1% Carbopol (MP4)

Structural deformation in constructs printed in 0.1% Carbopol (MP4)

Synchrotron movie capturing the details of the printed strands and their patterns (AVI)

■ AUTHOR INFORMATION

Corresponding Author

Vahid Serpooshan − *Wallace H. Coulter Department of Biomedical Engineering, Emory University School of Medicine and Georgia Institute of Technology, Atlanta, Georgia 30322, United States; Department of Pediatrics, Emory University, Atlanta, Georgia 30322, United States; Children's Healthcare of Atlanta, Atlanta, Georgia 30322, United States;* orcid.org/0000-0002-5304-095X; Email: vahid.serpooshan@emory.edu

Authors

Liqun Ning − *Wallace H. Coulter Department of Biomedical Engineering, Emory University School of Medicine and Georgia Institute of Technology, Atlanta, Georgia 30322, United States; Department of Pediatrics, Emory University, Atlanta, Georgia 30322, United States;* orcid.org/0000-0002-3651-7410

Riya Mehta − *Department of Biology, Emory University, Atlanta, Georgia 30322, United States*

Cong Cao − *Department of Physics, Emory University, Atlanta, Georgia 30322, United States*

Andrea Theus − *Wallace H. Coulter Department of Biomedical Engineering, Emory University School of Medicine and Georgia Institute of Technology, Atlanta, Georgia 30322, United States; Department of Pediatrics, Emory University, Atlanta, Georgia 30322, United States*

Martin Tomov − *Wallace H. Coulter Department of Biomedical Engineering, Emory University School of Medicine and Georgia Institute of Technology, Atlanta, Georgia 30322, United States; Department of Pediatrics, Emory University, Atlanta, Georgia 30322, United States*

Ning Zhu − *Canadian Light Source, Saskatoon S7N 2 V3, Saskatchewan, Canada*

Eric R. Weeks − *Department of Physics, Emory University, Atlanta, Georgia 30322, United States;* orcid.org/0000-0003-1503-3633

Holly Bauser-Heaton − *Department of Pediatrics, Emory University, Atlanta, Georgia 30322, United States; Children's Healthcare of Atlanta, Atlanta, Georgia 30322, United States; Sibley Heart Center at Children's Healthcare of Atlanta, Atlanta, Georgia 30322, United States*

Complete contact information is available at: https://pubs.acs.org/10.1021/acsami.0c15078

Notes

The authors declare no competing financial interest.

■ ACKNOWLEDGMENTS

This research was funded by the NIH grant number R00HL127295 and Emory University School of Medicine (Pediatric Research Alliance Pilot Grant and the Dean's Imagine, Innovate and Impact (I3) Research Award). The work of C.C. and E.R.W. was supported by the NSF grant number DMR-1609763. Part of the research described in this paper was performed at the Canadian Light Source, a national research facility of the University of Saskatchewan, which is supported by the Canada Foundation for Innovation (CFI), the Natural Sciences and Engineering Research Council (NSERC), the National Research Council (NRC), the Canadian Institutes of Health Research (CIHR), the Government of Saskatchewan, and the University of Saskatchewan. Also, we thank Drs. Shaoxiong Wu, Bing Wang, and Rui Liu for their technical support for the experiments.

■ REFERENCES

(1) Lee, K. Y.; Mooney, D. J. Hydrogels for tissue engineering. *Chem. Rev.* **2001**, *101* (7), 1869−1880.

(2) Ning, L.; Sun, H.; Lelong, T.; Guilloteau, R.; Zhu, N.; Schreyer, D. J.; Chen, D. X. 3D bioprinting of scaffolds with living Schwann cells for potential nerve tissue engineering applications. *Biofabrication* **2018**, *10* (3), 035014.
(3) Serpooshan, V.; Mahmoudi, M.; Hu, D. A.; Hu, J. B.; Wu, S. M. Bioengineering cardiac constructs using 3D printing. *Journal of 3D printing in medicine* **2017**, *1* (2), 123−139.
(4) Ning, L.; Chen, X. A brief review of extrusion-based tissue scaffold bio-printing. *Biotechnol. J.* **2017**, *12* (8), 1600671.
(5) Murphy, S. V.; Atala, A. 3D bioprinting of tissues and organs. *Nat. Biotechnol.* **2014**, *32* (8), 773−785.
(6) Gao, T.; Gillispie, G. J; Copus, J. S; Anil Kumar, P. R.; Seol, Y.-J.; Atala, A.; Yoo, J. J; Lee, S. J. Optimization of gelatin−alginate composite bioink printability using rheological parameters: A systematic approach. *Biofabrication* **2018**, *10* (3), 034106.
(7) Ning, L.; Xu, Y.; Chen, X.; Schreyer, D. J. Influence of mechanical properties of alginate-based substrates on the performance of Schwann cells in culture. *J. Biomater. Sci., Polym. Ed.* **2016**, *27* (9), 898−915.
(8) Ning, L.; Zhu, N.; Mohabatpour, F.; Sarker, M.; Schreyer, D. J.; Chen, X. Bioprinting Schwann cell-laden scaffolds from low-viscosity hydrogel compositions. *J. Mater. Chem. B* **2019**, *7* (29), 4538−4551.
(9) England, S.; Rajaram, A.; Schreyer, D. J.; Chen, X. Bioprinted fibrin-factor XIII-hyaluronate hydrogel scaffolds with encapsulated Schwann cells and their in vitro characterization for use in nerve regeneration. *Bioprinting* **2017**, *5*, 1−9.
(10) Schuurman, W.; Khristov, V.; Pot, M.; Van Weeren, P.; Dhert, W.; Malda, J. Bioprinting of hybrid tissue constructs with tailorable mechanical properties. *Biofabrication* **2011**, *3* (2), 021001.
(11) Kang, H.-W.; Lee, S. J.; Ko, I. K.; Kengla, C.; Yoo, J. J.; Atala, A. A 3D bioprinting system to produce human-scale tissue constructs with structural integrity. *Nat. Biotechnol.* **2016**, *34* (3), 312−319.
(12) Kolesky, D. B.; Truby, R. L.; Gladman, A. S.; Busbee, T. A.; Homan, K. A.; Lewis, J. A. 3D bioprinting of vascularized, heterogeneous cell-laden tissue constructs. *Adv. Mater.* **2014**, *26* (19), 3124−3130.
(13) Lin, N. Y.; Homan, K. A.; Robinson, S. S.; Kolesky, D. B.; Duarte, N.; Moisan, A.; Lewis, J. A. Renal reabsorption in 3D vascularized proximal tubule models. *Proc. Natl. Acad. Sci. U. S. A.* **2019**, *116* (12), 5399−5404.
(14) Lee, A.; Hudson, A.; Shiwarski, D.; Tashman, J.; Hinton, T.; Yerneni, S.; Bliley, J.; Campbell, P.; Feinberg, A. 3D bioprinting of collagen to rebuild components of the human heart. *Science* **2019**, *365* (6452), 482−487.
(15) Bhattacharjee, T.; Zehnder, S. M.; Rowe, K. G.; Jain, S.; Nixon, R. M.; Sawyer, W. G.; Angelini, T. E. Writing in the granular gel medium. *Science advances* **2015**, *1* (8), No. e1500655.
(16) Bhattacharjee, T.; Gil, C. J.; Marshall, S. L.; Urueña, J. M.; O'Bryan, C. S.; Carstens, M.; Keselowsky, B.; Palmer, G. D.; Ghivizzani, S.; Gibbs, C. P.; et al. Liquid-like solids support cells in 3D. *ACS Biomater. Sci. Eng.* **2016**, *2* (10), 1787−1795.
(17) Soltan, N.; Ning, L.; Mohabatpour, F.; Papagerakis, P.; Chen, X. Printability and cell viability in bioprinting alginate dialdehyde-gelatin scaffolds. *ACS Biomater. Sci. Eng.* **2019**, *5* (6), 2976−2987.
(18) Jin, Y.; Compaan, A.; Bhattacharjee, T.; Huang, Y. Granular gel support-enabled extrusion of three-dimensional alginate and cellular structures. *Biofabrication* **2016**, *8* (2), 025016.
(19) Yue, K.; Trujillo-De Santiago, G.; Alvarez, M. M.; Tamayol, A.; Annabi, N.; Khademhosseini, A. Synthesis, properties, and biomedical applications of gelatin methacryloyl (GelMA) hydrogels. *Biomaterials* **2015**, *73*, 254−271.
(20) Xiao, S.; Zhao, T.; Wang, J.; Wang, C.; Du, J.; Ying, L.; Lin, J.; Zhang, C.; Hu, W.; Wang, L.; et al. Gelatin methacrylate (GelMA)-based hydrogels for cell transplantation: an effective strategy for tissue engineering. *Stem Cell Rev. Rep.* **2019**, *15* (5), 664−679.
(21) McCormack, A.; Highley, C. B.; Leslie, N. R.; Melchels, F. P. 3D Printing in Suspension Baths: Keeping the Promises of Bioprinting Afloat. *Trends Biotechnol.* **2020**, *38* (6), 584−593.
(22) Billiet, T.; Gevaert, E.; De Schryver, T.; Cornelissen, M.; Dubruel, P. The 3D printing of gelatin methacrylamide cell-laden tissue-engineered constructs with high cell viability. *Biomaterials* **2014**, *35* (1), 49−62.
(23) Sun, W.; Starly, B.; Daly, A. C.; Burdick, J. A.; Groll, J.; Skeldon, G.; Shu, W.; Sakai, Y.; Shinohara, M.; Nishikawa, M.; et al. The bioprinting roadmap. *Biofabrication* **2020**, *12* (2), 022002.
(24) Gao, T.; Gillispie, G. J.; Copus, J. S.; Pr, A. K.; Seol, Y. J.; Atala, A.; Yoo, J. J.; Lee, S. J. Optimization of gelatin-alginate composite bioink printability using rheological parameters: a systematic approach. *Biofabrication* **2018**, *10* (3), 034106.
(25) Liu, W.; Heinrich, M. A.; Zhou, Y.; Akpek, A.; Hu, N.; Liu, X.; Guan, X.; Zhong, Z.; Jin, X.; Khademhosseini, A.et al., Extrusion Bioprinting of Shear-Thinning Gelatin Methacryloyl Bioinks. *Adv. Healthcare Mater.* **2017**, *6* (12) DOI: 10.1002/adhm.201770062.
(26) Koti, P.; Muselimyan, N.; Mirdamadi, E.; Asfour, H.; Sarvazyan, N. A. Use of GelMA for 3D printing of cardiac myocytes and fibroblasts. *Journal of 3D printing in medicine* **2019**, *3* (1), 11−22.
(27) Bhattacharjee, T.; Zehnder, S. M.; Rowe, K. G.; Jain, S.; Nixon, R. M.; Sawyer, W. G.; Angelini, T. E. Writing in the granular gel medium. *Sci. Adv.* **2015**, *1* (8), No. e1500655.
(28) Dimitriou, C. J.; Ewoldt, R. H.; McKinley, G. H. Describing and prescribing the constitutive response of yield stress fluids using large amplitude oscillatory shear stress (LAOStress). *J. Rheol.* **2013**, *57* (1), 27−70.
(29) Wang, L.; Xu, M. E.; Luo, L.; Zhou, Y.; Si, P. Iterative feedback bio-printing-derived cell-laden hydrogel scaffolds with optimal geometrical fidelity and cellular controllability. *Sci. Rep.* **2018**, *8* (1), 2802.
(30) Tomov, M. L.; Theus, A.; Sarasani, R.; Chen, H.; Serpooshan, V. 3D Bioprinting of Cardiovascular Tissue Constructs: Cardiac Bioinks. In *Cardiovascular Regenerative Medicine: Tissue Engineering and Clinical Applications*; Serpooshan, V., Wu, S. M., Eds.; Springer International Publishing: Cham, 2019; pp 63−77.
(31) Hu, J. B.; Tomov, M. L.; Buikema, J. W.; Chen, C.; Mahmoudi, M.; Wu, S. M.; Serpooshan, V. Cardiovascular tissue bioprinting: Physical and chemical processes. *Appl. Phys. Rev.* **2018**, *5* (4), 041106.
(32) Chen, X. B. Extrusion Bioprinting of Scaffolds for Tissue Engineering Applications. **2019** DOI: 10.1007/978-3-030-03460-3.
(33) Jin, Y.; Zhao, D.; Huang, Y. Study of extrudability and standoff distance effect during nanoclay-enabled direct printing. *Bio-Design and Manufacturing* **2018**, *1* (2), 123−134.
(34) Ning, L.; Guillemot, A.; Zhao, J.; Kipouros, G.; Chen, D. Influence of flow behavior of alginate-cell suspensions on cell viability and proliferation. *Tissue Eng., Part C* **2016**, *22* (7), 652−662.
(35) Ning, L.; Yang, B.; Mohabatpour, F.; Betancourt, N.; Sarker, M.; Papagerakis, P.; Chen, X. Process-induced cell damage: pneumatic versus screw-driven bioprinting. *Biofabrication* **2020**, *12* (2), 025011.
(36) Blaeser, A.; Duarte Campos, D. F.; Puster, U.; Richtering, W.; Stevens, M. M.; Fischer, H. Controlling shear stress in 3D bioprinting is a key factor to balance printing resolution and stem cell integrity. *Adv. Healthcare Mater.* **2016**, *5* (3), 326−333.
(37) Ning, L.; Betancourt, N.; Schreyer, D. J.; Chen, X. Characterization of cell damage and proliferative ability during and after bioprinting. *ACS Biomater. Sci. Eng.* **2018**, *4* (11), 3906−3918.
(38) Yu, Y.-Z.; Zheng, L.-L.; Chen, H.-P.; Chen, W.-H.; Hu, Q.-X. Fabrication of hierarchical polycaprolactone/gel scaffolds via combined 3D bioprinting and electrospinning for tissue engineering. *Adv. Manuf.* **2014**, *2* (3), 231−238.
(39) Wang, K. Die swell of complex polymeric systems. *Viscoelasticity-From theory to biological applications* **2012**, *1*, 77−96.
(40) Hinton, T. J.; Jallerat, Q.; Palchesko, R. N.; Park, J. H.; Grodzicki, M. S.; Shue, H.-J.; Ramadan, M. H.; Hudson, A. R.; Feinberg, A. W. Three-dimensional printing of complex biological structures by freeform reversible embedding of suspended hydrogels. *Science advances* **2015**, *1* (9), No. e1500758.
(41) Bertassoni, L. E.; Cardoso, J. C.; Manoharan, V.; Cristino, A. L.; Bhise, N. S.; Araujo, W. A.; Zorlutuna, P.; Vrana, N. E.; Ghaemmaghami, A. M.; Dokmeci, M. R.; et al. Direct-write bioprinting of cell-laden methacrylated gelatin hydrogels. *Biofabrication* **2014**, *6* (2), 024105.

(42) Ying, G.; Jiang, N.; Yu, C.; Zhang, Y. S. Three-dimensional bioprinting of gelatin methacryloyl (GelMA). *Bio-Design and Manufacturing* **2018**, *1* (4), 215−224.
(43) Jin, Y.; Compaan, A.; Chai, W.; Huang, Y. Functional nanoclay suspension for printing-then-solidification of liquid materials. *ACS Appl. Mater. Interfaces* **2017**, *9* (23), 20057−20066.
(44) Zhu, N.; Li, M.; Cooper, D.; Chen, X. Development of novel hybrid poly (l-lactide)/chitosan scaffolds using the rapid freeze prototyping technique. *Biofabrication* **2011**, *3* (3), 034105.
(45) Ravindran, S.; Kotecha, M.; Huang, C.-C.; Ye, A.; Pothirajan, P.; Yin, Z.; Magin, R.; George, A. Biological and MRI characterization of biomimetic ECM scaffolds for cartilage tissue regeneration. *Biomaterials* **2015**, *71*, 58−70.
(46) Tanter, M.; Fink, M. Ultrafast imaging in biomedical ultrasound. *IEEE transactions on ultrasonics, ferroelectrics, and frequency control* **2014**, *61* (1), 102−119.
(47) Izadifar, Z.; Honaramooz, A.; Wiebe, S.; Belev, G.; Chen, X.; Chapman, D. Low-dose phase-based X-ray imaging techniques for in situ soft tissue engineering assessments. *Biomaterials* **2016**, *82*, 151−167.
(48) Serpooshan, V.; Quinn, T. M.; Muja, N.; Nazhat, S. N. Hydraulic permeability of multilayered collagen gel scaffolds under plastic compression-induced unidirectional fluid flow. *Acta Biomater.* **2013**, *9* (1), 4673−80.
(49) Serpooshan, V.; Quinn, T. M.; Muja, N.; Nazhat, S. N. Characterization and modelling of a dense lamella formed during self-compression of fibrillar collagen gels: implications for biomimetic scaffolds. *Soft Matter* **2011**, *7* (6), 2918−2926.
(50) Serpooshan, V.; Julien, M.; Nguyen, O.; Wang, H.; Li, A.; Muja, N.; Henderson, J. E.; Nazhat, S. N. Reduced hydraulic permeability of three-dimensional collagen scaffolds attenuates gel contraction and promotes the growth and differentiation of mesenchymal stem cells. *Acta Biomater.* **2010**, *6* (10), 3978−87.
(51) Tibbitt, M. W.; Anseth, K. S. Hydrogels as extracellular matrix mimics for 3D cell culture. *Biotechnol. Bioeng.* **2009**, *103* (4), 655−663.
(52) Chaudhuri, O.; Gu, L.; Klumpers, D.; Darnell, M.; Bencherif, S. A.; Weaver, J. C.; Huebsch, N.; Lee, H.-P.; Lippens, E.; Duda, G. N.; et al. Hydrogels with tunable stress relaxation regulate stem cell fate and activity. *Nat. Mater.* **2016**, *15* (3), 326−334.
(53) Miermont, A.; Lee, S. W. L.; Adriani, G.; Kamm, R. D. Quantitative screening of the effects of hyper-osmotic stress on cancer cells cultured in 2-or 3-dimensional settings. *Sci. Rep.* **2019**, *9* (1), 1−10.
(54) Li, M.; Tian, X.; Schreyer, D. J.; Chen, X. Effect of needle geometry on flow rate and cell damage in the dispensing-based biofabrication process. *Biotechnol. Prog.* **2011**, *27* (6), 1777−1784.
(55) Noshadi, I.; Hong, S.; Sullivan, K. E.; Shirzaei Sani, E.; Portillo-Lara, R.; Tamayol, A.; Shin, S. R.; Gao, A. E.; Stoppel, W. L.; Black, L. D., III; et al. In vitro and in vivo analysis of visible light crosslinkable gelatin methacryloyl (GelMA) hydrogels. *Biomater. Sci.* **2017**, *5* (10), 2093−2105.
(56) Shirahama, H.; Lee, B. H.; Tan, L. P.; Cho, N.-J. Precise tuning of facile one-pot gelatin methacryloyl (GelMA) synthesis. *Sci. Rep.* **2016**, *6* (1), 1−11.
(57) Stratesteffen, H.; Köpf, M.; Kreimendahl, F.; Blaeser, A.; Jockenhoevel, S.; Fischer, H. GelMA-collagen blends enable drop-on-demand 3D printablility and promote angiogenesis. *Biofabrication* **2017**, *9* (4), 045002.
(58) Chen, X.; Li, M.; Ke, H. Modeling of the flow rate in the dispensing-based process for fabricating tissue scaffolds. *Journal of Manufacturing Science and Engineering* **2008**, *130* (2), 021003.
(59) Vogelgesang, M.; Farago, T.; Morgeneyer, T. F.; Helfen, L.; dos Santos Rolo, T.; Myagotin, A.; Baumbach, T. Real-time image-content-based beamline control for smart 4D X-ray imaging. *J. Synchrotron Radiat.* **2016**, *23* (5), 1254−1263.
(60) Paganin, D.; Mayo, S. C.; Gureyev, T. E.; Miller, P. R.; Wilkins, S. W. Simultaneous phase and amplitude extraction from a single defocused image of a homogeneous object. *J. Microsc.* **2002**, *206* (1), 33−40.
(61) Serpooshan, V.; Julien, M.; Nguyen, O.; Wang, H.; Li, A.; Muja, N.; Henderson, J. E.; Nazhat, S. N. Reduced hydraulic permeability of three-dimensional collagen scaffolds attenuates gel contraction and promotes the growth and differentiation of mesenchymal stem cells. *Acta Biomater.* **2010**, *6* (10), 3978−3987.
(62) Zhao, X.; Sun, X.; Zhang, J.; Bai, B. Gel composition and brine concentration effect on hydrogel dehydration subjected to uniaxial compression. *J. Pet. Sci. Eng.* **2019**, *182*, 106358.
(63) Lee, S.; Serpooshan, V.; Tong, X.; Venkatraman, S.; Lee, M.; Lee, J.; Chirikian, O.; Wu, J. C.; Wu, S. M.; Yang, F. Contractile force generation by 3D hiPSC-derived cardiac tissues is enhanced by rapid establishment of cellular interconnection in matrix with muscle-mimicking stiffness. *Biomaterials* **2017**, *131*, 111−120.
(64) Serpooshan, V.; Muja, N.; Marelli, B.; Nazhat, S. N. Fibroblast contractility and growth in plastic compressed collagen gel scaffolds with microstructures correlated with hydraulic permeability. *J. Biomed. Mater. Res., Part A* **2011**, *96A* (4), 609−620.

https://dx.doi.org/10.1021/acsami.0c15078
ACS Appl. Mater. Interfaces 2020, 12, 44563−44577